# Supporting Information

Kramer *et al.* 10.1073/pnas.0801967105

## SI Materials and Methods

**Preparation of Oocytes and Nuclei.** Female *Xenopus* laevis were anesthetized with 0.1% ethyl *m*-aminobenzoate methanesulfonate (Serva) and their ovaries were removed. Oocytes were dissected from ovary clusters and stored in HRF buffer (87 mM NaCl, 6.3 mM KCl, 1 mM $MgCl_2$, 1.5 mM $CaCl_2$, 10 mM Hepes, 100 units/100 $\mu$g penicillin/streptomycin; pH 7.4) before use. For isolation of the cell nuclei, the oocytes were transferred into nuclear isolation medium (NIM) composed of 90 mM KCl, 26 mM NaCl, 5.6 mM $MgCl_2$ (corresponding to a free $Mg^{2+}$ concentration of 2 mM), 1.1 mM EGTA, and 10 mM Hepes; and titrated to pH 7.4. We added 1.5% polyvinylpyrrolidone (PVP, $M_r$ = 40,000; Sigma) to compensate for the lack of macromolecules in the NIM, mimicking the intact cytosol. The presence of PVP is crucial to prevent the swelling (more than 100% in the absence of PVP) of total nuclear volume that occurs instantaneously after isolation in pure electrolyte solution.

**Preparation of Nuclear Envelopes.** After placing the oocytes in NIM, we manually isolated the nuclei by piercing the oocyte with two pincers. Individual intact nuclei were picked up with a Pasteur pipette and transferred to a glass coverslip placed under a stereomicroscope. The chromatin was then carefully removed by using sharp needles, and the nuclear envelope was spread on 3-aminopropyltriethoxysilane (APTES)-coated glass with the nucleoplasmic side facing downwards. APTES was purchased from Sigma, and the coating was performed according to the method described by Howarter *et al.* (1). Samples which were used for force volume measurements were kept unfixed. The other samples were fixed by using 2% glutaraldehyde and 1% paraformaldehyde for 1 h at room temperature, washed three times with NIM, and investigated with AFM without any drying procedure.

**Microinjection of Cytochrome *c*.** Typically, 50 nl aqueous solution of cytochrome *c* (Sigma), was microinjected into each oocyte by using a microinjector (OocytePipetl; Drummond), resulting in a final concentration of 10 $\mu$M. For calculation of the final intracellular concentration of injected cytochrome *c*, the cytosolic volume of an oocyte was taken to be $\approx$1 $\mu$l. After injection of cytochrome *c*, oocytes were incubated at 18°C for the indicated times.

**Assay of DEVDase Activity in Oocyte Cell-Free Extracts.** Collagenase (Sigma) at a concentration of 1 mg/ml dissolved in HRF was used to defolliculate oocytes. A time equal to 2.5 h after the injection of cytochrome *c* (NIM for controls), 50 oocytes were crushed by centrifugation at 15,000 $\times$ g. The clear supernatant was diluted 10-fold with PBS and incubated at room temperature for about 30 min in the presence of 10 mM DTT. Ac-DEVD-AFC (Biomol), dissolved in DMSO, was added to a final concentration of 10 $\mu$g/ml. Fluorescence was measured in a flourimeter (Fluroscan II, MTX Lab Systems; excitation, 385 nm; emission, 515 nm).

**Antibodies.** The antibody against the N terminus of Nup153 (2) was a kind gift by Ian Mattaj (EMBL, Heidelberg, Germany). The anti-Nup358 antibody (3) was generously provided by Mary Dasso (Laboratory of Gene Regulation and Development, NICHD/NIH, Bethesda, USA). We are obliged to Douglass Forbes (University of California, San Diego, USA) for providing the anti-Tpr antibody (4). The anti-Lamin B antibody (X223) was purchased from Progen, and the Mab414 was from Covance. Peroxidase-labeled secondary antibodies were purchased from Dianova.

**Western Blot Analysis.** Fifty nuclei were prepared for each point in time (60 min, 150 min, and 240 min) after injection of cytochrome *c*. Controls (0 min) were injected with an equal volume of NIM. Nuclei were briefly washed in NIM and subsequently centrifuged at 15,000 *g*. The pellets were washed two times in NIM, and 40 $\mu$l of NIM was added to the pellets.

Ten microliters of a 5 $\times$ SDS-DTT sample loading buffer (0.5 M Tris, 8.5% SDS, 27.5% sucrose, 100 mM DTT, 0.03% bromophenol blue) was added. Proteins were solubilized and denaturated by heating the mixture to 95°C for 5 min. Then the samples were put on ice for 1 min and were centrifuged at 15,000 $\times$ *g* to remove debris. Samples were kept at $-$20°C. Volumes equivalent to five nuclei were resolved on 10% SDS polyacrylamide gels. Subsequently, proteins were transferred onto nitrocellulose membranes (Schleicher & Schüll) by electroblotting. Membranes were incubated in blocking solution [5% skim milk powder in TBS-T (1 $\times$ TBS, pH. 7.4 containing 0.05% Tween-20)] overnight at 4°C. Subsequently, blots were incubated with the respective primary antibody for 1 h at room temperature (4°C). After washing (6 $\times$ 5 min with TBS-T) and incubation with appropriate peroxidase-labeled secondary antibody for 1 h at room temperature, membranes were washed again. Finally, proteins were detected by using a highly sensitive chemiluminescence substrate (Pierce SuperSignal West Femto, Perbio Science).

**AFM.** The application of AFM to nuclear envelopes has been described in detail elsewhere (5). We used a Multimode atomic force microscope (with a NanoScope V controller; Veeco) equipped with an optical microscope, a videocamera, and a monitor to visualize the nuclear envelope and the AFM tip on its stage. We used standard V-shaped 100-$\mu$m-long silicon nitride cantilevers with a spring constant of 0.08 N/m and pyramidal tips with an estimated tip diameter of 10 nm (Olympus). The images were recorded in tapping mode, with 512 lines per screen and a scan rate of 1.5 Hz. The forces applied during the scanning procedure were minimized by retracting the AFM tip until it lost contact with the sample surface, and reengaging the tip at an amplitude set point (i.e., force value) as close as possible to the lift-off value. Although the AFM tip physically interacts with the nuclear envelope, the repeatability of results from multiple scans indicated that the preparation was not damaged. Moreover, scanning at low forces (3 nN or less) left no visible marks in the preparation.

**Data Analysis and Image Processing.** AFM images were analyzed by using SPIP software (Image Metrology)

**Force Curves, Force-Volume Measurements, and Stiffness Maps.** A simple force curve records the force felt by the AFM tip as it approaches and retracts from a point on the sample surface. A force volume contains an array of force curves over the entire sample area. Each force curve is measured at a unique *x-y* position in the area, and force curves from an array of *x-y* points are combined into a three-dimensional array, or "volume," of force data. The value at a point (*x*,*y*,*z*) in the volume is the deflection (force) on the cantilever at that position in space. The force applied to the sample can be set constant for each *x-y* point

by the so-called trigger threshold, which also defines the return point of the AFM-tip after each approach. The height detected at this point is recorded and produces the height image of a force-volume measurement. The settings for the force-volume measurements were as follows: Number of samples was 128 × 128 × 128 ($x$,$y$,$z$), scan rate was 9 Hz (force curves/ sec), and the trigger threshold was set to 310 pN. Soft cantilevers with a spring constant of 0.01 N/m were used (MSCT; Veeco). Spring constants were determined experimentally by the thermal noise method (6). All curves of a force-volume measurement were analyzed automatically with the free software PUNIAS (http://site.voila.fr/punias/). PUNIAS first calculates a force-indentation curve for each force curve by using the experimentally derived spring constant. The initial slope of a given force-indentation curve represents the stiffness of the sample at the corresponding $x$-$y$ point. A linear fitting, covering the data points of the first 25 nm of indentation, was applied in the analysis of each curve. From the analysis of the force-indentation curves, color-coded stiffness maps can be generated.

**Statistical Analyses.** Data are presented as the mean ± standard error of the mean (SEM). In each experimental series (solvent and cytochrome *c*), 10 nuclei were isolated. Statistical significance of mean values was tested with the unpaired Student's $t$ test. $P$ value was always 0.001 or less. In the analyses of the stiffness maps, the SPIP program was used to remove the stiffness values of the nuclear pore-containing areas. Next, the mean stiffness was calculated for each of the 128 lines of the maps. These mean stiffness values were used for the unpaired Student's $t$ test.


1. Howarter J-A, Youngblood J-P (2006) Optimization of silica silanization by 3-aminopropyltriethoxysilane. *Langmuir* 22:11142–11147.
2. Walther T-C, *et al.* (2001) The nucleoporin Nup153 is required for nuclear pore basket formation, nuclear pore complex anchoring and import of a subset of nuclear proteins. *EMBO J* 20:5703–5714.
3. Joseph J, Liu S-T, Jablonski S-A, Yen T-J, Dasso M (2004) The RanGAP1-RanBP2 complex is essential for microtubule-kinetochore interactions in vivo. *Curr Biol* 14:611–617.
4. Shah S, Tugendreich S, Forbes D (1998) Major binding sites for the nuclear import receptor are the internal nucleoporin Nup153 and the adjacent nuclear filament protein Tpr. *J Cell Biol* 141:31–49.
5. Danker T, Mazzanti M, Tonini R, Rakowska A, Oberleithner H (1997) Using atomic force microscopy to investigate patch-clamped nuclear membrane. *Cell Biol Int* 21:747–757.
6. Florin E-L, Moy V-T, Gaub H-E (1994) Adhesion forces between individual ligand-receptor pairs. *Science* 264:415–417.

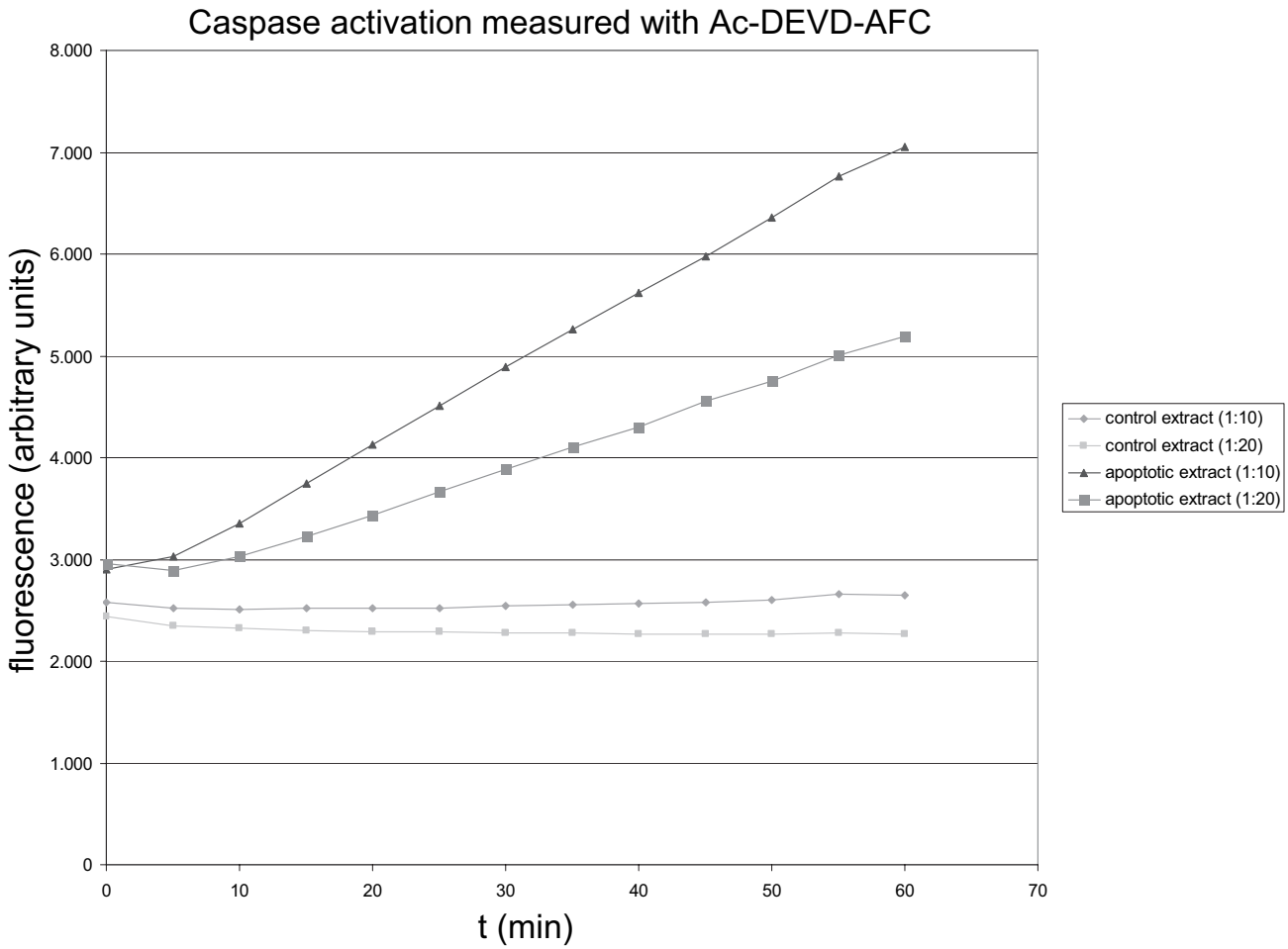


**Fig. S1.** Assay of DEVDase activity in *Xenopus laevis* oocyte extracts. Ac-DEVD-AFC was added to a final concentration of ≈150 nM. The release of AFC after hydrolysis of the substrate is monitored at 515 nm; on excitation, at 385 nm. The extracts were prepared from 10–20 oocytes ≈2.5 h after injection of cytochrome *c*. The final intracellular concentration of cytochrome *c* was 10 $\mu$M.

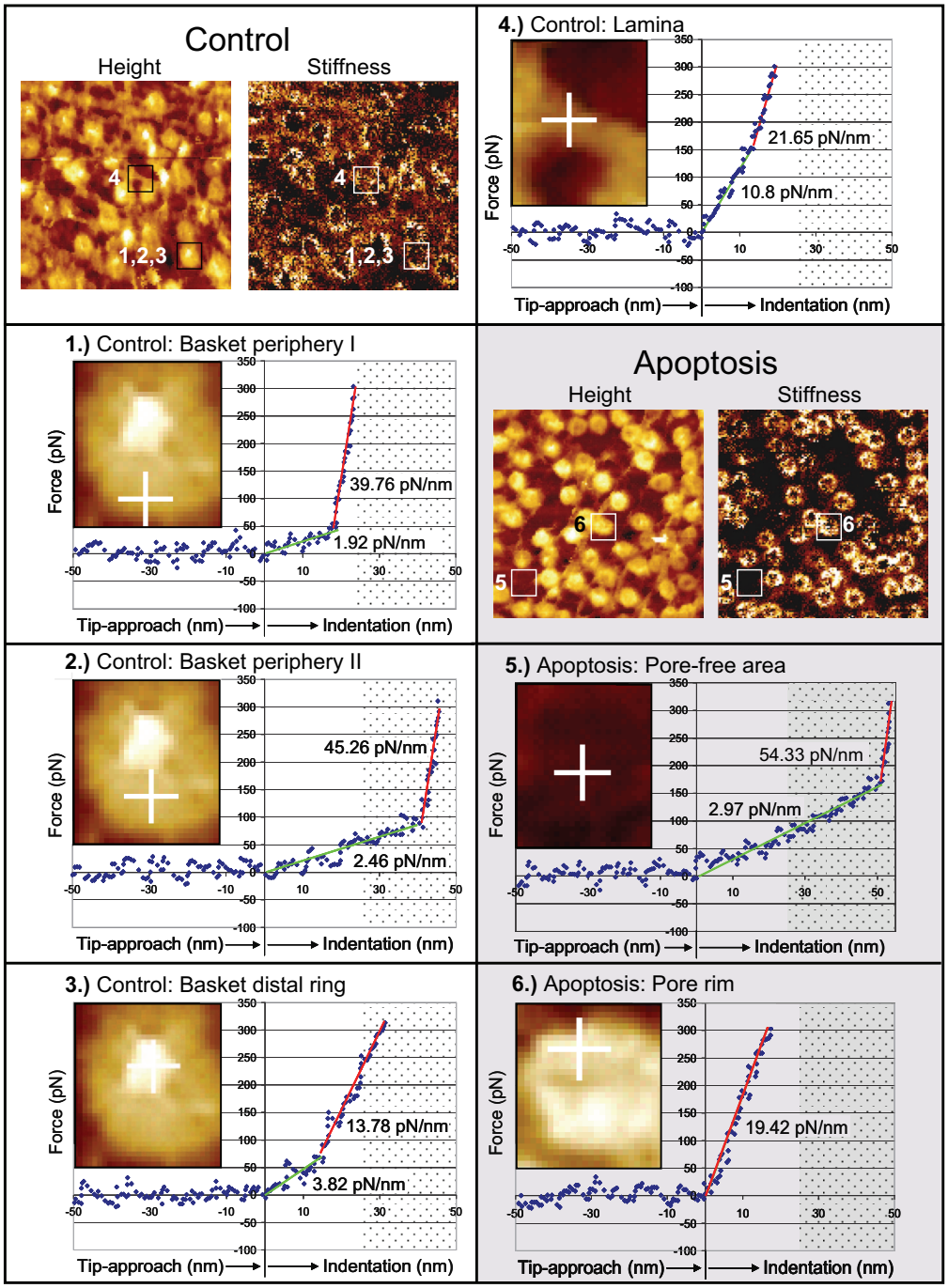


**Fig. S2.** Exemplary force-indentation curves from apoptotic and control NEs. Height images and stiffness maps of control and apoptotic NEs provide an overview on the origin of the force-indentation curves. In each diagram, the area where the force curve was taken is shown in the *Inset*, and the exact position is marked with a white cross. Because the stiffness maps were obtained by applying a linear fitting over the first 25 nm of indentation, the areas representing a deeper indentation are marked with dots. (*Inset 1*) Basket periphery indented: Two slopes can be observed. In the first ≈14 nm (first slope, green) the soft basket filaments are pressed down until they reach the more rigid nucleoplasmic ring of the NPC, which causes the second slope (red). (*Inset 2*) Near the center (distal ring) of the basket: Two slopes can still be observed, and the first slope is elongated. The basket or a basket filament (first slope, green) is pressed downwards ≈40 nm until the underlying, more rigid nucleoplasmic ring is reached (second slope, red). (*Inset 3*) On the distal ring: Two slopes can still be observed. The first (≈12 nm indentation, green) is probably caused by filamentous material on top of the basket. It is followed by a steeper slope (red) that could represent the collective resistance of all 8 basket filaments taken together. (*Inset 4*) On a fiber of the nuclear lamina: A relatively steep slope is observed (green) that becomes even steeper after ≈12 nm indentation (red), possibly when further, underlying fibers are compressed and pressed on. (*Inset 5*) On an NPC-free area of the apoptotic NE (nuclear lamina degraded): A gentle slope (≈50 nm indentation, green), is likely to be due to a compression of the periplasmic space between the inner and the outer nuclear membranes; a steeper slope (red) is probably caused by a direct compression of the two membranes. (*Inset 6*) On an NPC rim of an apoptotic NE: The single slope displayed is relatively steep and is probably caused by the rigid nucleoplasmic ring, which becomes directly accessible after the loss of the basket. However, it is interesting to note that this slope is less steep than the second slope of control NPCs, which could be due to a degradation of components of the inner NPC core structure.